Biomaterials Science

PAPER

View Article Online
View Journal | View Issue

Cite this: *Biomater. Sci.*, 2019, **7**, 125

A high-density collagen xerogel thread prevents the progression of peritoneal fibrosis

Shigehisa Aoki, *[a] Toshiaki Takezawa, *[b] Kei Nagase, [a,c] Ayumi Oshikata-Mitazaki, [b] Sayuri Morito,[a] Takehisa Sakumoto,[a] Masanori Masuda,[a] Mihoko Yamamoto-Rikitake, [a] Takashi Akutagawa[a,d] and Shuji Toda[a]

Peritoneal fibrosis is often provoked by peritoneal dialysis and is an essential precursor condition to the development of encapsulating peritoneal sclerosis. This study aimed to determine the efficacy of a high-density collagen xerogel thread (CXT) for the prevention of peritoneal fibrosis. Female ICR mice received intraperitoneal injections of chlorhexidine gluconate (CG) every other day to induce peritoneal fibrosis. For evaluation, the insertion of CXT or infusion of atelocollagen gel into the peritoneal cavity was conducted on the day before CG injection. For comparison, no collagen treatment after CG injection, and abdominal puncture without CG injection were also performed. Peritoneal fibrosis and inflammation were significantly suppressed by CXT for a long period. CXT prevented mesothelial epithelial–mesenchymal transition, myofibroblast emergence, and inflammatory cell invasion in the peritonitis tissue. In the early phase, atelocollagen gel modulated the expression of the fibrosis-associated protein transforming growth factor (TGF)-β, connective tissue growth factor (CTGF), and CD105 in the peritoneum under CG-induced inflammation, while CXT did not. In contrast, CXT regulated the expression of CTGF and CD105 in the late phase and maintained antimicrobial protein REG3G at the same level as the Sham group in the early and late phases. Although the precise mechanism remains to be clarified, these findings suggest that CXT may have the potential to be developed as a simple therapeutic device to prevent peritoneal fibrosis, a severe complication in patients undergoing long-term peritoneal dialysis.

Received 14th May 2018,
Accepted 30th October 2018

DOI: 10.1039/c8bm00536b

rsc.li/biomaterials-science

Introduction

Fibroproliferative diseases reflect a fatal tissue-remodeling state provoked by acute or chronic inflammation in various tissues and organs.[1] Peritoneal fibrosis is often triggered by peritoneal dialysis (PD) and is an essential precursor condition to the development of encapsulating peritoneal sclerosis.[2] This serious complication leads to a high mortality rate in PD patients.[3] To date, various methods and materials have been explored in attempts to prevent peritoneal fibrosis, but there is no established standard therapeutic method for this condition.[4,5]

A collagen xerogel in xerotes is fabricated by sufficient drying of a collagen vitrigel.[6] Collagen vitrigel is a collagen-based biomaterial composed of high-density collagen fibrils equivalent to connective tissues *in vivo*, and is prepared by three processes: gelation of collagen sol, vitrification of collagen gel, and rehydration of vitrified collagen gel.[7] We established several shapes of collagen xerogel and vitrigel devices such as plane membranes,[8] spherical surface membranes,[9] and dome-shaped membranes.[10] Collagen vitrigel devices possess excellent biocompatibility, high mechanical strength, and good permeability for proteins with high molecular weights.[10,11] Previously, we utilized the characteristics of collagen xerogel to establish an artificial skin[12] and an esophageal stricture prevention device.[13] We demonstrated that these two devices can inhibit scar formation and inflammation in damaged tissue and promote the epithelization of the regenerative area. Notably, these devices also inhibit the emergence of myofibroblasts in the damaged area in similar manners.

The peritoneum is composed of a mesothelial layer and a submesothelial interstitial layer (SMIL), with an abdominal musculature located beneath the SMIL. The progression of fibrosis involves excess interstitial hypercellularity and matrix

[a]*Department of Pathology and Microbiology, Faculty of Medicine, Saga University, Saga, Japan. E-mail: aokis@cc.saga-u.ac.jp; Fax: +81-952-34-2055; Tel: +81-952-34-2231*
[b]*Division of Biotechnology, Institute of Agrobiological Sciences, National Agriculture and Food Research Organization, Ibaraki, Japan. E-mail: t.takezawa@affrc.go.jp; Fax: +81-29-838-6294; Tel: +81-29-838-6294*
[c]*Department of Urology, Faculty of Medicine, Saga University, Saga, Japan*
[d]*Department of Internal Medicine and Gastrointestinal Endoscopy, Faculty of Medicine, Saga University, Saga, Japan*

accumulation in the SMIL.[14] It is recognized that myofibroblasts are the most important cell component for interstitial matrix accumulation and consequent structural deformation associated with fibrosis.[15] During the process for wound healing and progressive fibrosis, fibroblasts and other cells transform into myofibroblasts that express alpha-smooth muscle actin (α-SMA) and synthesize mesenchymal cell-related matrix proteins.[16] In PD, epithelial–mesenchymal transition (EMT) of peritoneal mesothelial cells is recognized as an important cell source of myofibroblasts.[17]

In this study, we used two advantages of collagen vitrigel, *i.e.*, prevention of myofibroblast emergence and flexible workability, to develop a new anti-fibrotic device, a collagen xerogel thread (CXT), for inflammatory disorder of the peritoneum. The purpose of the study was to assess the potential of CXT as a simple insertion device for the peritoneal cavity by evaluating the extent to which it can prevent peritoneal fibrosis under inflammatory conditions.

Experimental section

Thread type of collagen xerogel

Atelocollagen is a collagen type with low immunogenic potential that is obtained by the removal of the N- and C-terminal telopeptide components,[18] which are recognized to induce antigenicity. A raw material of 0.5% atelocollagen sol was prepared by uniformly mixing equal volumes of 1.0% acidic solution of porcine-derived atelocollagen for regenerative medicine (Nippon Meat Packers Inc., Tokyo, Japan) and a serum-free culture medium. Columnar collagen gels were formed in plastic pipettes for 1-, 2-, and 5 ml volume specifications by gelation after pouring 1.4, 2.8, and 7.0 ml of the porcine-derived atelocollagen sol, respectively (Fig. 1A). Each fragile columnar collagen gel was gently removed from the pipette and linearly placed on a flat vinyl sheet. The gels were irradiated with UV light (254 nm) at 800 mJ cm^{-2}, inverted, and irradiated with UV at the same dose to enhance the gel strength (Fig. 1B). The UV-irradiated columnar collagen gels were vitrified by hanging from one end on a line (Fig. 1C and D). Fragile collagen vitrigel threads (CVTs) were prepared by rehydrating the vitrified gels in a thread shape with phosphate-buffered saline (Fig. 1E). The CVTs were re-vitrified by carefully hanging from one end on a line to obtain CXTs (Fig. 1F and G). The CXTs were linearly placed on a flat vinyl sheet, irradiated with UV light at 400 mJ cm^{-2}, inverted, and irradiated with UV at the same dose to enhance the mechanical strength (Fig. 1H). Subsequently, 17 cm pieces with an almost uniform thickness were cut from the CXTs derived from the 1-, 2-, and 5 ml volume pipettes as CXT1, CXT2, and CXT5, respectively. The final amounts of atelocollagen in CXT1, CXT2, and CXT5 were 5.9, 10.7, and 24.0 mg, respectively. CXT1, CXT2, and CXT5 were used for histological analyses (Fig. 2A and B), and CXT2 was used for protein analyses.

Animal model

Animals were housed in the animal facilities of Saga University under specific pathogen-free conditions, maintained at 25 °C on a 12 h light/dark cycle (lights on at 08:00), and had free access to food and water. The protocol for all animal experiments was approved by the Animal Experimentation Committee of Saga University. Procedures involving mice and their care conformed to international guidelines, as described in Principles of Laboratory Animal Care (National Institutes of Health publication 85-23, revised 1985). Six-week-old female ICR mice weighing 26–30 g (Nippon SLC Ltd, Osaka, Japan) were used. Peritoneal fibrosis was induced by intraperitoneal injection of 0.1% chlorhexidine gluconate (CG) in 15% ethanol dissolved in saline, as described previously.[19,20] Mice received injections of CG into the peritoneal cavity at a volume of 10 mL per kg body weight every other day (CG group) (Fig. 2C). The CG injection was moved one day earlier in the cases for protein extraction at days 7 and 35.

In the Gel group, atelocollagen gel (Nippon Meat Packers Inc.), an ingredient of CXT, was infused into the peritoneum on the day before CG injection. The maximum infusion volume of atelocollagen gel was set at 2.2 ml, because volumes of ice-chilled gel exceeding 2.2 ml could easily induce hypothermia in infused mice.

In the CXT group, one CXT was inserted into the peritoneum in each mouse on the day before CG injection. Each CXT was grasped with tweezers and inserted through an

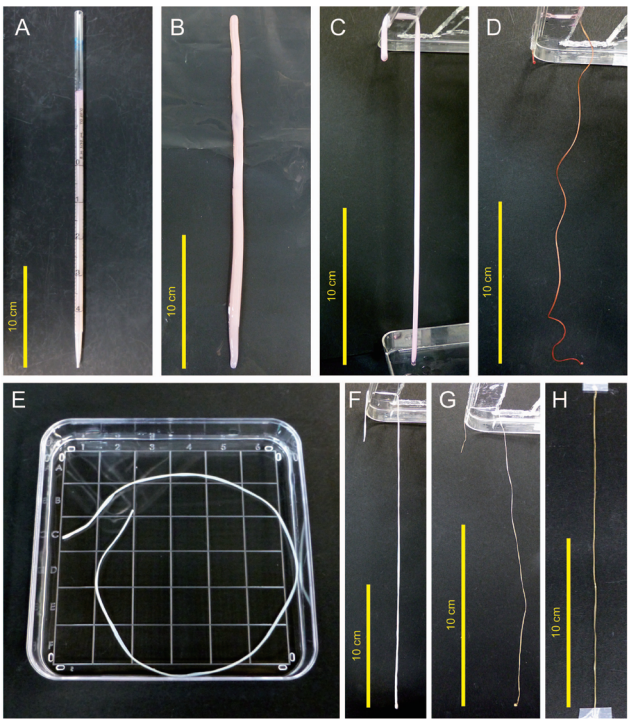

Fig. 1 Procedure for CXT (collagen xerogel thread) preparation. A, Columnar collagen gel formed in a plastic pipette for the 5 ml volume specification. B, UV-irradiated columnar collagen gel. C, Columnar collagen gel hung for vitrification. D, Vitrified columnar collagen gel. E, CVT (collagen vitrigel thread) under rehydration. The grid size on the plastic dish is 1.3 cm. F, CVT hung for vitrification. G, Vitrified CVT, *i.e.* CXT. H, UV-irradiated CXT.

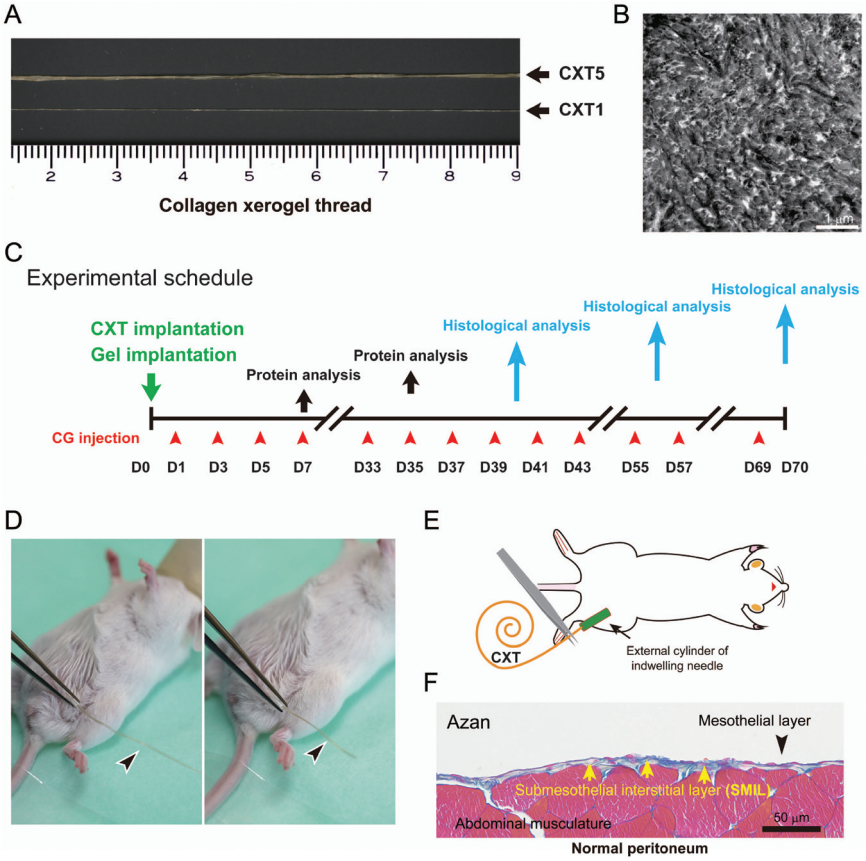

Fig. 2 CXTs, experimental schedule, and normal peritoneum. A, Collagen xerogel threads CXT5 and CXT1. B, Ultrastructure of a CXT cross-section. The transmission electron micrograph shows that coarse collagen fibrils are concentrated in a very dense state. C, Schematic of the experimental schedule. D, The CXT (arrowhead) is grasped with tweezers and inserted through an external cylinder. E, Schematic and actual implantation of CXT. F, Normal parietal peritoneum. The SMIL (arrow) is a thin zone between the mesothelial layer (arrowhead) and the abdominal musculature in the normal state.

indwelling needle on the day before CG injection (Fig. 2D and E). The CXT was converted into a CVT, a rehydrated form of CXT, by interstitial fluid and blood plasma in the mouse body. In the control group, the abdominal wall was punctured by using an indwelling needle without CG treatment. All animal groups contained 3–5 mice.

Histology and immunohistochemistry

After 40, 56, and 70 days of continuing CG injection, abdominal wall and small intestine samples were collected. Histological examinations were performed by hematoxylin–eosin (HE) and Azan staining. Tissues and CXTs were fixed with 10% formalin, routinely processed, and embedded in paraffin. HE and Azan staining procedures were subsequently performed on deparaffinized sections. To examine the ultrastructure, tissues were fixed with 2.5% glutaraldehyde and 1% osmic acid, dehydrated with alcohol, and embedded in epoxy resin. Thin sections were observed using an electron microscope (JME 2100; Jeol Ltd, Tokyo, Japan).

Immunohistochemistry was performed by a standard method. For the identification of mesothelial EMT, a mouse monoclonal anti-pan-cytokeratin (CK AE1/AE3) antibody (Dako, Glostrup, Denmark), a mouse monoclonal anti-vimentin antibody (Abcam, Cambridge, UK), and a rabbit polyclonal anti-N-cadherin antibody (Abcam) were used. A rabbit polyclonal anti-connective tissue growth factor (CTGF) antibody (Proteintech, Rosemont, IL, USA) was used to detect fibrosis-related tissue reactions. Myofibroblasts, leukocytes, and macrophages were respectively detected with a mouse monoclonal anti-α-SMA antibody (Dako), a rabbit polyclonal anti-CD45 antibody (Abcam), and a rabbit monoclonal anti-F4/80 antibody (Abcam). Proliferative cells were labeled with a mouse monoclonal anti-proliferating cell nuclear antigen (PCNA) antibody (Dako). To detect REG3G, a rabbit polyclonal anti-REG3G antibody (Abcam) was used. Immunostaining was performed at room temperature using a Dako autostainer (Dako). As negative controls, phosphate-buffered saline, normal mouse IgG, and normal rabbit IgG were used as appropriate instead of a primary antibody.

Morphometric analysis

We measured the SMIL thickness above the abdominal muscle in cross-sections of the abdominal wall (Fig. 2F). The thickness was measured at 10 points in each of the five randomly chosen non-contiguous and non-overlapping areas (low magnification,

×10 objective) in Azan-stained sections by a standard method.[14] To evaluate the degrees of inflammation and stromal cell proliferation in the regenerative tissue, the numbers of CD45-positive, F4/80-positive, and PCNA-positive cells were measured in five randomly chosen non-contiguous and non-overlapping areas at hot spots (high magnification, ×40 objective) in the stained sections.

Western blotting

For western blotting analysis, peritoneum samples were collected after 7 and 35 days of treatment. The harvested tissues were placed in Laemmli buffer, fractionated by 10% SDS-PAGE, transferred to PVDF membranes, and incubated with anti-transforming growth factor (TGF)-β (Cell Signaling Technology, Danvers, MA, USA), anti-CTGF (Proteintech), and anti-REG3G (Abcam) primary antibodies. The bound antibodies on the membranes were visualized using WesternBreeze reagents (Invitrogen, Carlsbad, CA, USA). The densities of the bands were determined using a FUSION system (Vilber-Lourmat, Eberhardzell, Germany) and analyzed with the Image J software.[21] The results were presented as ratios relative to the control values.

Statistical analysis

Data obtained from 3–5 independent experiments were analyzed by Tukey's test or Wilcoxon's test depending on the results for the equality of variance. Values are presented as mean ± SD. Values of $p < 0.05$ were considered to indicate statistically significant differences. Mean values of replicates in the experiments were used to determine statistical significance. All statistical analyses were performed using JMP 13 for Windows (SAS, Cary, NC, USA).

Results and discussion

CXT prevents peritoneal fibrosis in mice with CG-induced peritonitis

Peritoneal fibrosis was induced in mice by the intraperitoneal injection of 0.1% CG in 15% ethanol dissolved in saline every other day.[19,20] In the Gel1 group, 1.2 ml of atelocollagen gel was infused into the peritoneal cavity on the day before CG injection. The CXT1 group was inserted with the CXT made from 1.2 ml of atelocollagen on the day before CG injection. The inserted CXT was converted into a CVT, a rehydrated form of CXT, by the interstitial fluid in the peritoneal cavity within a short period of time. The CG group underwent puncture of the peritoneal wall and treatment with a collagen device on the day before CG injection. The Sham group was treated with one abdominal puncture on the day before CG injection in another group. Fig. 2C shows a brief description of the CXT preparation and experimental procedures.

First, we analyzed the anti-fibrotic effect of CXT on CG-induced peritonitis. The CG-untreated Sham group showed a transparent peritoneum and normal branching vessel structure at day 40 (Fig. 3A1 and A2). In the CG group, the peritoneum exhibited a murky white color and an obscure branching vessel structure arising from peritoneal fibrosis (Fig. 3B1 and B2). The peritoneum in the Gel1 group showed a slight white color and comparatively sharply defined branching vessels (Fig. 3C1 and C2). Fibrotic adhesion between the small intestine and peritoneum was seen in the CG (Fig. 3B2) and Gel1 (Fig. 3C2) groups. In contrast, the CXT1 group had a transparent peritoneal wall and sharply defined branching vessel structure (Fig. 3D1 and D2).

Histologically, the Sham group had a relatively thin SMIL in the parietal (Fig. 3A3 and A5) and visceral (Fig. 3A4) peritoneum. The CG group had a highly thickened fibrous peritoneum associated with inflammatory cells in the submesothelial layer of the parietal peritoneum, and fibrin deposition was observed on the surface of the parietal peritoneum (Fig. 3B3 and B5). The visceral peritoneum also had a thickened submesothelial layer with small numbers of inflammatory cells in the CG group (Fig. 3B4).

The SMIL thickening and hypercellularity induced by CG were suppressed by atelocollagen gel infusion and CXT insertion. In the Gel1 group, the fibrosis of the SMIL in the parietal (Fig. 3C3 and C5) and visceral (Fig. 3C4) peritoneum was thinner compared with that in the CG group. The CXT1 group exhibited less fibrotic SMILs in the parietal (Fig. 3D3 and D5) and visceral (Fig. 3D4) peritoneum. Compared with the CG and Gel1 groups, the CXT1 group showed thinner submesothelial layers in the parietal and visceral peritoneum wherein fibrotic change was prevented. The SMIL thicknesses were evaluated in Azan-stained sections of parietal peritoneum samples. The thicknesses in the groups were: Sham, 4.95 ± 1.48 μm; CG, 333.10 ± 82.03 μm; Gel1, 113.43 ± 37.78 μm; CXT1, 23.53 ± 13.68 μm (Fig. 3E).

The Gel1 group exhibited the migration of fibroblasts from the contacting submesothelial layer to the residual atelocollagen gel, with some fibroblasts infiltrating the central part of the atelocollagen gel (Fig. 3F). In the CXT1 group, fibroblasts infiltrated into only the marginal area of the CVT, the rehydrated form of CXT, at day 40 (Fig. 3G). Fibrotic adhesions of the parietal peritoneum to the intestinal wall and between adjacent intestinal walls were observed in the CG group (Fig. 3H and I).

CXT prevents fibrosis in mice with CG-induced peritonitis during 56 days

We further analyzed the anti-fibrotic effect of CXT on peritonitis over a long period. CXT5 was made from 5.4 ml of atelocollagen and its length was 17 cm. As body weight loss was observed in the CG group mice at day 56, we did not perform observations of the CG group beyond 56 days in consideration of humane treatment of the experimental animals.

Owing to the severe fibrotic adhesion between the small intestine and parietal peritoneum in the CG group, the laparotomy process was difficult. In the CG group, the peritoneum exhibited a grayish-white color and an indeterminable branching vessel structure (Fig. 4A1, A2, B1, and B2). In contrast, the CXT5 group showed a transparent peritoneal wall with a slight

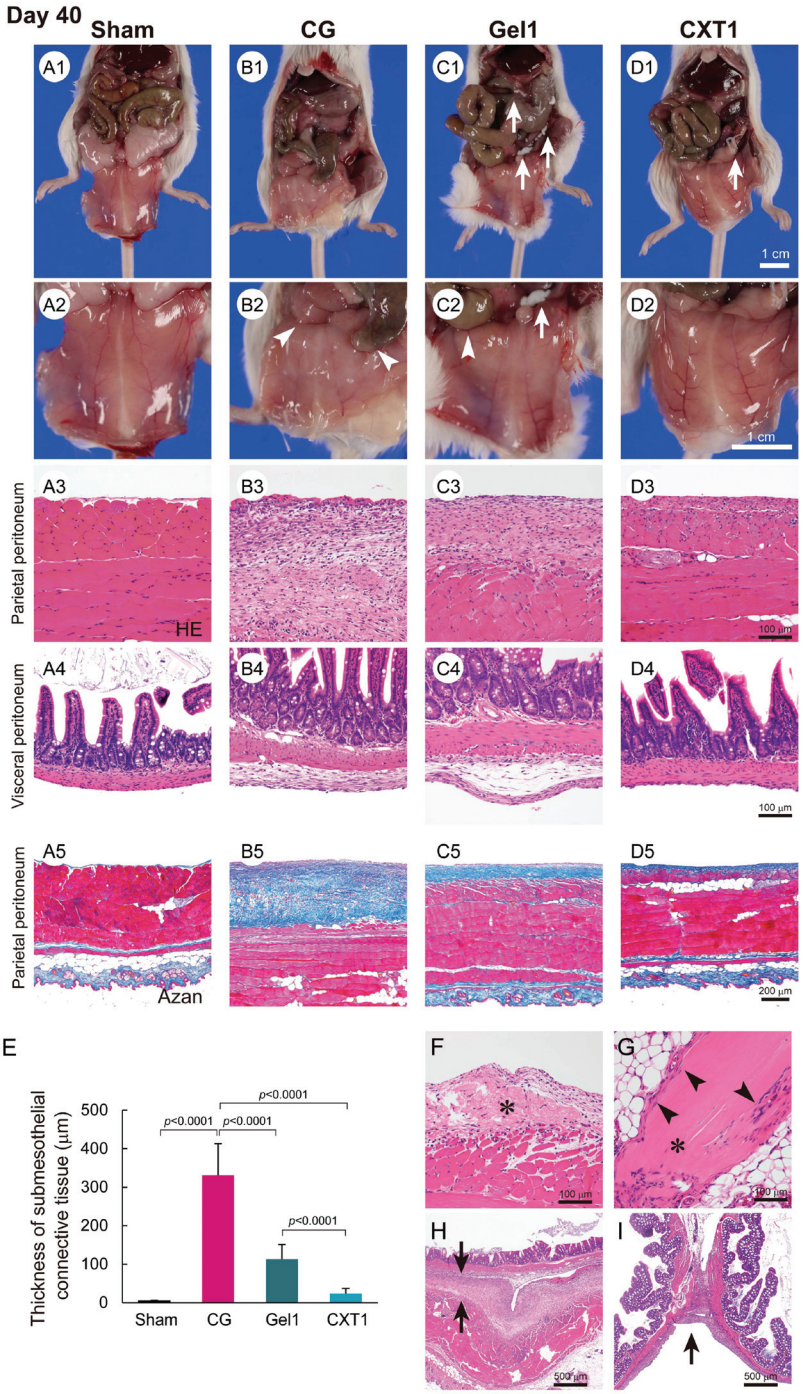

Fig. 3 Macroscopic and microscopic findings of the peritoneum at day 40. A1–A2, The Sham group shows a normal transparent peritoneal wall and sharply defined branching vessel structure in the parietal peritoneum. B1–B2, The CG group shows a murky white color and an obscure branching vessel structure in the parietal peritoneum. The arrowheads in B2 indicate fibrotic adhesion between the small intestine and peritoneum. C1–C2, The Gel1 group has a slight white color and comparatively sharply defined branching vessels in the parietal peritoneum. The arrows in C1 and C2 indicate the residual implanted atelocollagen gel. The arrowhead in C2 indicates fibrotic adhesion between the small intestine and peritoneum. D1–D2, The CXT1 group exhibits a transparent peritoneal wall and sharply defined branching vessel structure like the Sham group. The arrow in D1 indicates the residual CVT. A3–A5, The Sham group shows a thin SMIL in the parietal and visceral peritoneum. B3 and B5, The CG group shows a highly thickened fibrous peritoneum associated with inflammatory cells and fibrin deposition. B4, The visceral peritoneum also has a thickened SMIL. C3–C5, The fibrosis in the parietal and visceral peritoneum of the Gel1 group is thinner than that in the CG group. D3–D5, The CXT1 group exhibits thin SMILs in the parietal and visceral peritoneum. E, Parietal peritoneum thicknesses. The mean thicknesses were: Sham, 4.95 ± 1.48 μm; CG, 333.10 ± 82.03 μm; Gel1, 113.43 ± 37.78 μm; CXT1, 23.53 ± 13.68 μm. F, Fibroblasts have infiltrated the central part of the atelocollagen gel (asterisk). G, Fibroblasts have infiltrated the marginal area of the CVT (arrowheads). The asterisk indicates the residual CVT. H, The arrows indicate the fibrotic adhesion of the parietal peritoneum to the visceral peritoneum of the intestine in the CG group. I, Fibrotic adhesion of the adjacent intestinal tracts in the CG group (arrow).

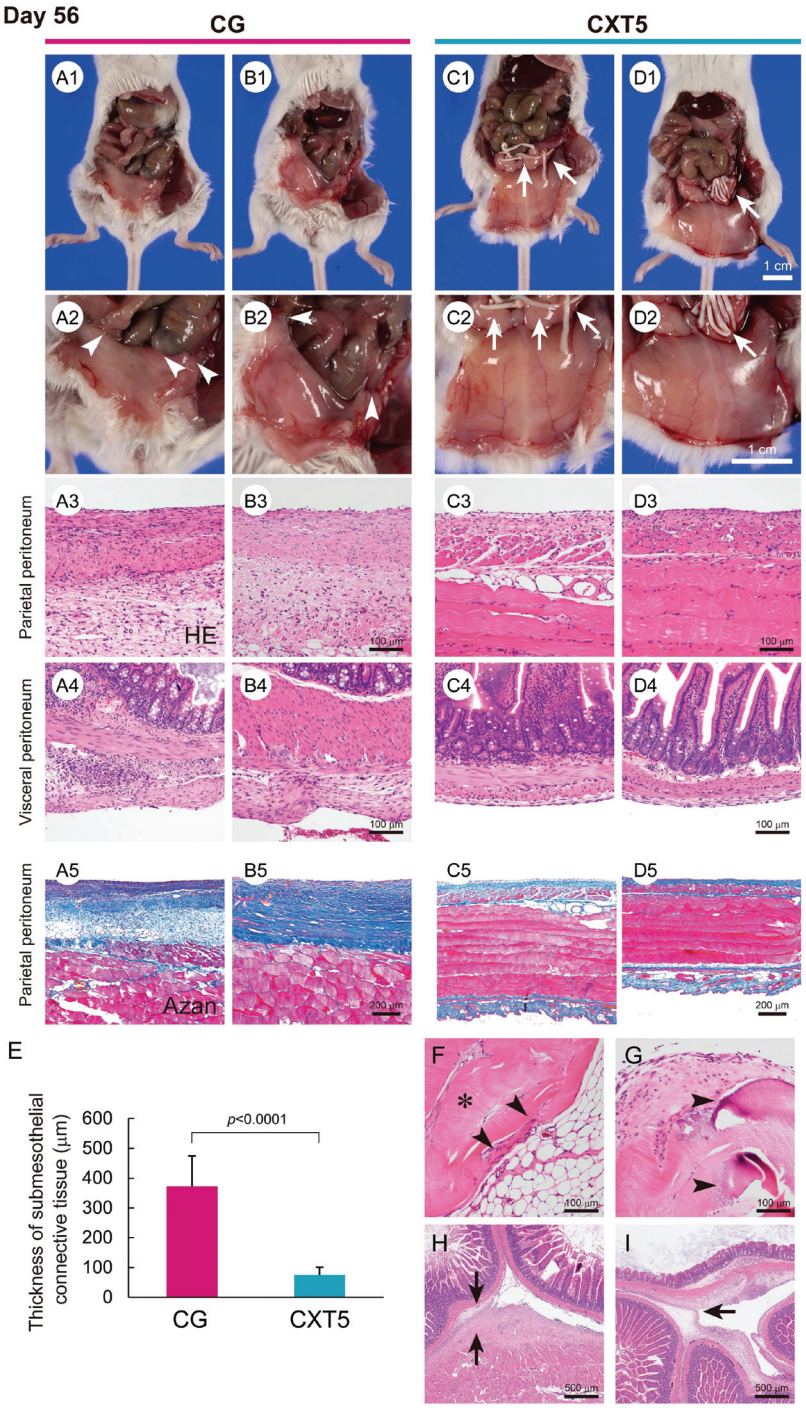

Fig. 4 Macroscopic and microscopic findings of the peritoneum at day 56. A1–A2 and B1–B2, The CG group exhibits a grayish white color and an indeterminable branching vessel structure in the parietal peritoneum. The arrowheads in A2 and B2 indicate the fibrotic adhesion of adjacent intestinal tracts. C1–C2 and D1–D2, The CXT5 group shows a transparent peritoneal wall with precise visualization of branching vessels. The arrows in C2 and D2 indicate the residual CVTs. A3, A5, B3, and B5, The CG group shows a highly thickened fibrous change associated with inflammatory cells in the SMIL of the parietal peritoneum. C3, C5, D3, and D5, The CXT5 group exhibits a thinner fibrous SMIL in the parietal peritoneum. A4 and B4, The CG group shows a thickened fibrous change associated with inflammatory cells in the SMIL of the visceral peritoneum. C4 and D4, The CXT5 group exhibits a thinner fibrous SMIL in the visceral peritoneum. E, Parietal peritoneum thicknesses. The mean thicknesses were: CG, 372.01 ± 102.01 μm; CXT5, 74.85 ± 26.03 μm. F, Infiltration of fibroblasts (arrowheads) into the CVT (asterisk) is limited to the marginal area. Foreign-body reactions to the CVT are undetectable. G, The CVT in the insertion site of the parietal peritoneum shows mild collagen degeneration (arrowheads). H, The arrows indicate fibrotic adhesion of the parietal peritoneum to the visceral peritoneum of the intestine in the CG group. I, The arrow indicates the fibrotic adhesion of the adjacent intestinal walls in the CG group.

whitish color, and precise visualization of branching vessels at day 56 (Fig. 4C1, C2, D1, and D2).

Histological examination revealed a highly thickened fibrous change associated with inflammatory cells in the SMIL of the parietal (Fig. 4A3, A5, B3 and B5) and visceral (Fig. 4A4 and B4) peritoneum in the CG group. In contrast, the CXT5 group exhibited a thinner fibrous layer in the submesothelial zone of the parietal (Fig. 4C3, C5, D3 and D5) and visceral (Fig. 4C4 and D4) peritoneum compared with the CG group. The thickness of the SMIL in the parietal peritoneum was 372.01 ± 102.01 μm in the CG group and 74.85 ± 26.03 μm in the CXT5 group (Fig. 4E).

Fibroblast infiltration was localized to the marginal area (Fig. 4F), and limited collagen degeneration (Fig. 4G) was observed in the CVT at day 56. Foreign-body reactions to the CVT were not detected. The massive fibrotic adhesion of the peritoneum to the intestinal tract wall and between bordering intestinal tracts was observed in the CG group (Fig. 4H and I).

Atelocollagen gel and CXT show different outcomes in mice with CG-induced peritonitis

We performed a long-term evaluation of the differences between the gel form and the xerogel form in the anti-fibrotic effects and the outcomes of peritonitis. The Gel2 group was infused with 2.2 ml of atelocollagen gel into the peritoneal cavity, and the CXT2 group was inserted with a 17 cm CXT made from 2.2 ml of atelocollagen into the peritoneal cavity on the day before CG injection. As shown in Fig. 5A1, B1, and C1, the mice in the Gel2 and CXT2 groups showed lower adipose tissue mass compared with those in the Sham group at day 70. In the Gel2 group, the peritoneum exhibited a grayish-white color and an indeterminable branching vessel structure (Fig. 5B1). In contrast, the CXT2 group showed a transparent peritoneal wall with a mild whitish color and precise visualization of branching vessels (Fig. 5C1 and C3). Histological examination revealed a highly thickened fibrous change in the SMIL of the parietal peritoneum in the Gel2 group (Fig. 5D2). In contrast, the CXT2 group exhibited a thinner fibrous layer in the SMIL of the parietal peritoneum compared with the Gel2 group (Fig. 5D3). Fibroblast infiltration was observed only in the marginal area of the CXT (Fig. 5E).

Electron microscopic examination revealed that the Gel2 group exhibited fibroblast migration into the residual atelocollagen gel at day 70. Fine collagen fibrils produced by fibroblasts were mingled with coarse collagen fibrils of atelocollagen (Fig. 5F). In the CXT2 group, fibroblasts infiltrated into the marginal area of the CVT and the fine collagen fibrils produced by the fibroblasts were clearly demarcated from the coarse collagen fibrils of the CVT (Fig. 5G). There was a clear border between the fine and coarse collagen fibrils. In the residual CVT, the remaining collagen fibrils were smaller and thinner than those in the center area.

CXT prevents mesothelial EMT, myofibroblast emergence, and fibrosis-related protein expression

Next, we evaluated mesothelial EMT by intermediate filament (cytokeratin and vimentin) and adhesion molecule (N-cadherin) expression. As shown in Fig. 6, the Sham and CXT1 groups demonstrated CK AE1/AE3 expression in the surface-covering mesothelial cells. In contrast, the CG and Gel1 groups exhibited few CK AE1/AE3-positive cells in the fibrous area. The overlying mesothelial cells showed weak vimentin expression in the Sham group. Vimentin-positive mesenchymal cells were observed in the fibrous SMIL of the CG and Gel1 groups. In the CXT1 group, vimentin-positive mesenchymal cells were observed in the surface layers. N-Cadherin-positive cells were observed in the fibrous SMIL of the CG group. The Gel1 group had weak N-cadherin-positive cells in the surface layers. Very small numbers of N-cadherin-positive cells were detected in the Sham and CXT1 groups.

Regarding fibrosis-associated protein expression, the Sham group showed weak CTGF and scant α-SMA expression in the surface of the peritoneum. The CG group exhibited large numbers of CTGF-positive stromal cells and high proportions of α-SMA-positive stromal cells throughout the full thickness of the fibrous SMIL. In contrast, the Gel1 group had sparsely distributed CTGF-positive and α-SMA-positive stromal cells throughout the SMIL and in the surface layers. The CXT1 group had markedly small numbers of CTGF-positive and α-SMA-positive cells in the SMIL compared with the CG and Gel1 groups.

CXT inhibits inflammation and stromal cell proliferation

HE staining and immunostaining for CD45 (common leukocyte marker) and F4/80 (macrophage marker) revealed that the major inflammatory cells infiltrating the SMIL in the CG, Gel1, and CXT1 groups at day 40 were lymphocytes and macrophages, together with small numbers of neutrophils (Fig. 7). The numbers of CD45-positive and F4/80-positive cells in the CXT1 group were significantly lower than those in the CG and Gel1 groups. The Gel1 group showed significantly lower numbers of CD45-positive and F4/80-positive cells than the CG group. In the SMIL, the CXT1 group exhibited a significantly lower PCNA-positive ratio in the fibrous stroma compared with the other groups. The PCNA-positive ratio in the SMIL was significantly lower in the Gel1 group than in the CG group.

Collagen-based materials modulate the expression of fibrosis-associated and homeostatic proteins in distinctive manners

TGF-β, CTGF, and CD105 are known to be involved in pathological fibrotic responses.[22,23] In this experiment, we used a gel made from 2.2 ml of atelocollagen for the Gel2 group and a collagen thread made from 2.2 ml of atelocollagen for the CXT2 group. As shown in Fig. 8A, TGF-β expression in the CG and CXT2 groups was significantly higher than that in the Sham and Gel2 groups at day 7. CTGF expression in the CG and CXT2 groups was significantly lower than that in the

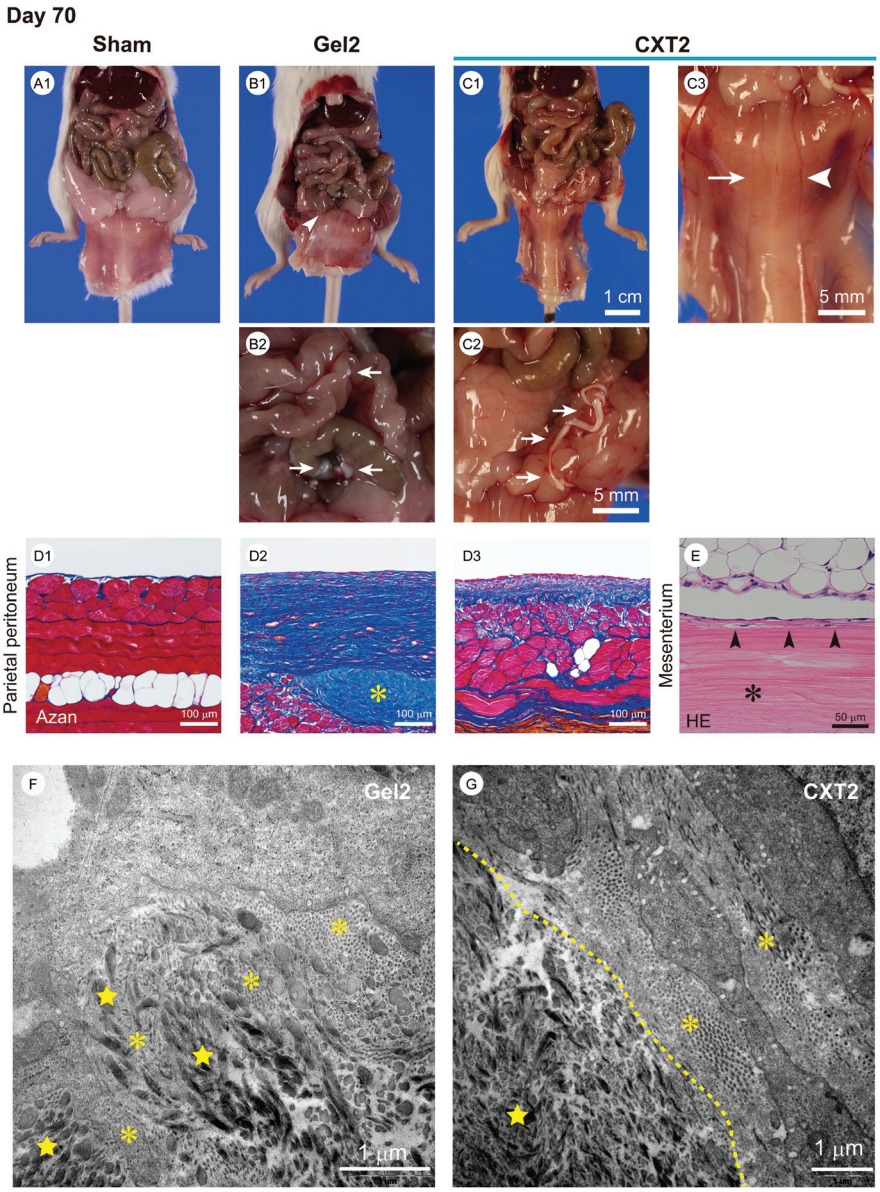

Fig. 5 Macroscopic and microscopic findings of the peritoneum, and electron microscopic findings of the atelocollagen gel and CVT at day 70. A1, The Sham group shows a normal transparent peritoneal wall and sharply defined branching vessel structure in the parietal peritoneum. Mature adipose tissue is observed. B1–B2, The Gel2 group exhibits a grayish white color and an indeterminable branching vessel structure in the parietal peritoneum. The arrowhead in B1 indicates fibrotic adhesion between the small intestine and the peritoneum. The arrows in B2 indicate the residual implanted atelocollagen gel. C1–C3, The CXT2 group shows a transparent peritoneal wall with precise visualization of branching vessels in the parietal peritoneum. The arrows in C2 indicate the residual CVT. A vessel adjacent to the CVT (arrowhead in C3) shows better translucency than a non-adjacent vessel (arrow in C3). D1, Azan staining shows a thin SMIL of the parietal peritoneum in the Sham group. D2, A highly thickened fibrous change is observed in the SMIL of the parietal peritoneum in the Gel2 group. The asterisk indicates the residual atelocollagen gel. D3, The fibrosis in the parietal peritoneum of the CXT2 group is thinner than that in the CG group. D4, The asterisk indicates the residual CVT. Small numbers of fibroblasts have infiltrated the marginal area of the CVT (arrowheads). E, Electron microscopic findings in the Gel2 group. At day 70, fine collagen fibrils (asterisks) produced by fibroblasts and coarse collagen fibrils (stars) of atelocollagen are mingled in the Gel2 group. F, Electron microscopic findings in the CXT2 group. In the CXT2 group, fibroblasts have infiltrated the marginal area of the CVT and a border between the fine collagen fibrils (asterisks) and coarse collagen fibrils (star) is observed at day 70. The dotted line indicates the boundary line between the coarse fibrils of the CVT and the fine fibrils produced by fibroblasts.

Sham and Gel2 groups. The Gel2 group showed significantly higher expression of CD105 compared with the Sham and CG groups. REG3G is an antimicrobial protein expressed in the gastrointestinal tract.[24] REG3G is expected to have a protective role against bacterial infection and translocation. REG3 lectins are known to restrict the access of bacteria to the intestinal epithelium.[25] REG3G expression in the CXT2 group was significantly higher than that in the CG group, with no differ-

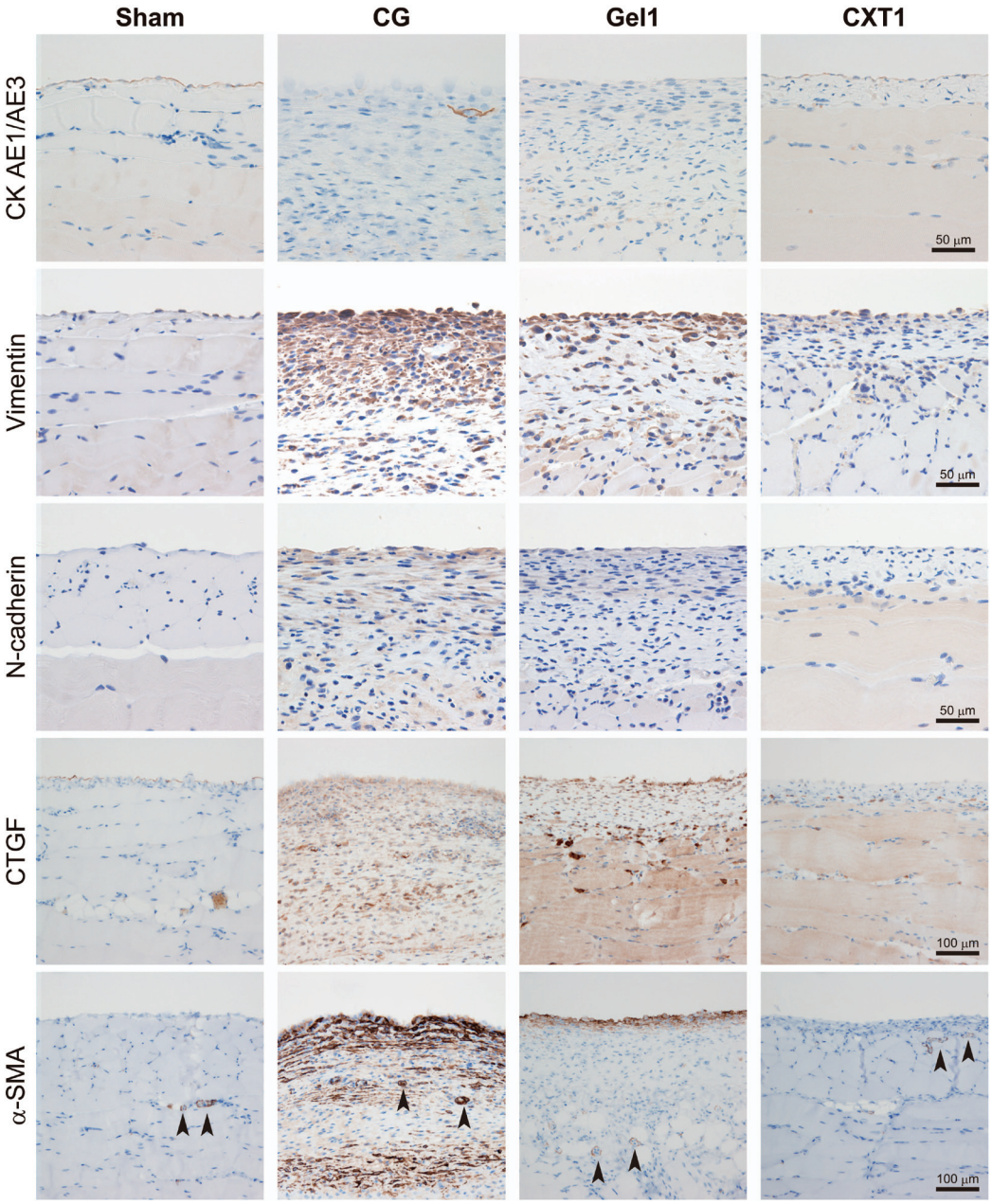

Fig. 6 Immunostaining of EMT and fibrosis-related markers. The Sham and CXT1 groups exhibit CK AE1/AE3 expression in the surface-covering mesothelial cells. The CG and Gel1 groups show very small numbers of CK AE1/AE3-positive cells in the fibrous area. The overlying mesothelial cells show vimentin expression in the Sham group. The CG and Gel1 groups have many vimentin-positive mesenchymal cells in the fibrous SMIL. In the CXT1 group, vimentin-positive mesenchymal cells are distributed in the surface layers. The CG group shows N-cadherin-positive cells in the thickened SMIL. The Gel1 group has weak N-cadherin-positive cells in the SMIL. Very small numbers of N-cadherin-positive cells are detected in the Sham and CXT1 groups. The Sham group shows CTGF and scant α-SMA expression in the surface of the peritoneum. The CG group exhibits large numbers of CTGF-positive cells, and high proportions of α-SMA-positive cells in the fibrous SMIL. The Gel1 group shows small numbers of CTGF-positive cells. α-SMA-positive stromal cells are distributed in the surface layers. The CXT1 group exhibits markedly small numbers of CTGF-positive and α-SMA-positive cells in the SMIL compared with the CG and Gel1 groups. Pericytes (arrowheads) show positivity for α-SMA.

ences in REG3G expression among the Sham, Gel2, and CXT2 groups at day 7.

At day 35, there were no significant differences in TGF-β expression among the groups. The CG group showed the highest CTGF expression, while the CXT group exhibited significantly lower CTGF expression compared with the other groups, similar to the immunostaining findings. The CG group showed significantly higher expression of CD105 compared with the Sham and CXT groups. REG3G expression was the highest in the CG group, while the CXT group had significantly lower REG3G expression than the Gel2 group.

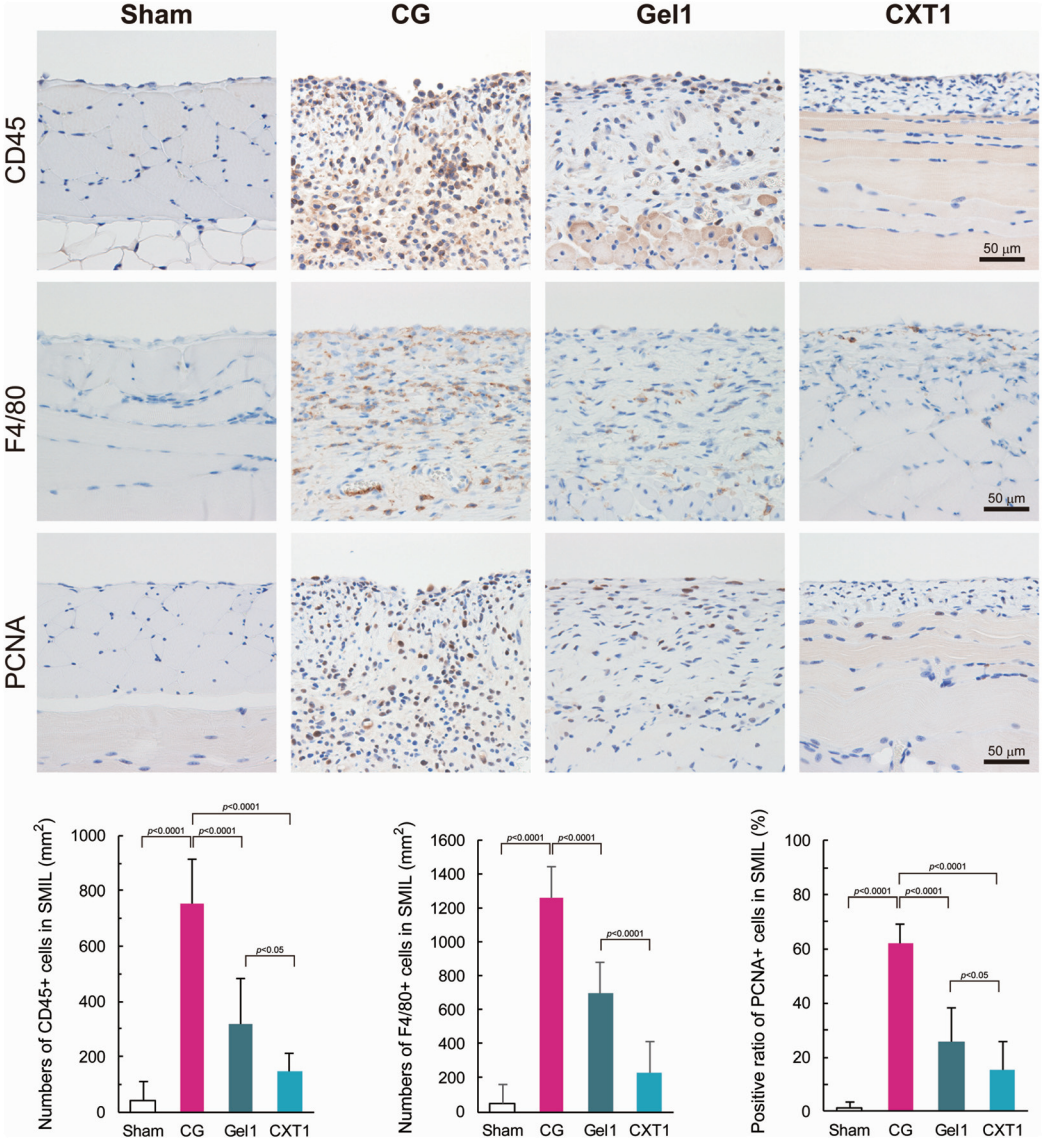

Fig. 7 Immunostaining of inflammation and stromal cell proliferation markers. The CG and Gel1 groups show the CD45-positive leukocyte and F4/80-positive macrophage infiltration of the SMIL. The numbers of CD45-positive and F4/80-positive cells are the highest in the CG group, followed by the Gel1 and CXT1 groups in that order at day 40. The CXT1 group exhibits a significantly lower PCNA-positive ratio in the fibrous stroma compared with the other groups. No significant differences in the numbers of CD45-positive, F4/80-positive, and PCNA-positive cells are observed between the Sham and CXT1 groups.

CXT inhibits REG3G expression in the parietal and visceral peritoneum in mice with CG-induced peritonitis

As shown in Fig. 9, REG3G-expressing cells in the parietal peritoneum were scant, and epithelial cells in the small intestinal mucosa showed weak expression of REG3G in the Sham and Gel1 groups at day 40. In the CG group, mesenchymal cells exhibited positivity for REG3G in the fibrotic area in both the parietal and visceral peritoneum. In the Gel1 group, mesenchymal cells expressed REG3G in the surface area of the thickened SMIL. In the small intestine, epithelial cells in the Sham, Gel1, and CXT1 groups and some smooth muscle cells in the Gel1 group showed weak expression of REG3G. Mesenchymal cells in the surface area of the visceral peritoneum also exhibited REG3G expression.

Not only PD, but also abdominal surgery can sometimes cause peritoneal fibrosis and intestinal adhesion.[25,26] The formation of postoperative adhesions in the peritoneum and intestine is a frequently encountered complication after gynecological and general abdominal surgery, and has significant clinical and economic consequences. Many interventions have been trialed to prevent this pathological tissue remodeling in the peritoneal cavity, but no standard method has been established.[27,28]

TGF-β and CTGF are ubiquitously expressed in various types of tissue fibrosis, including fibrotic diseases, and they

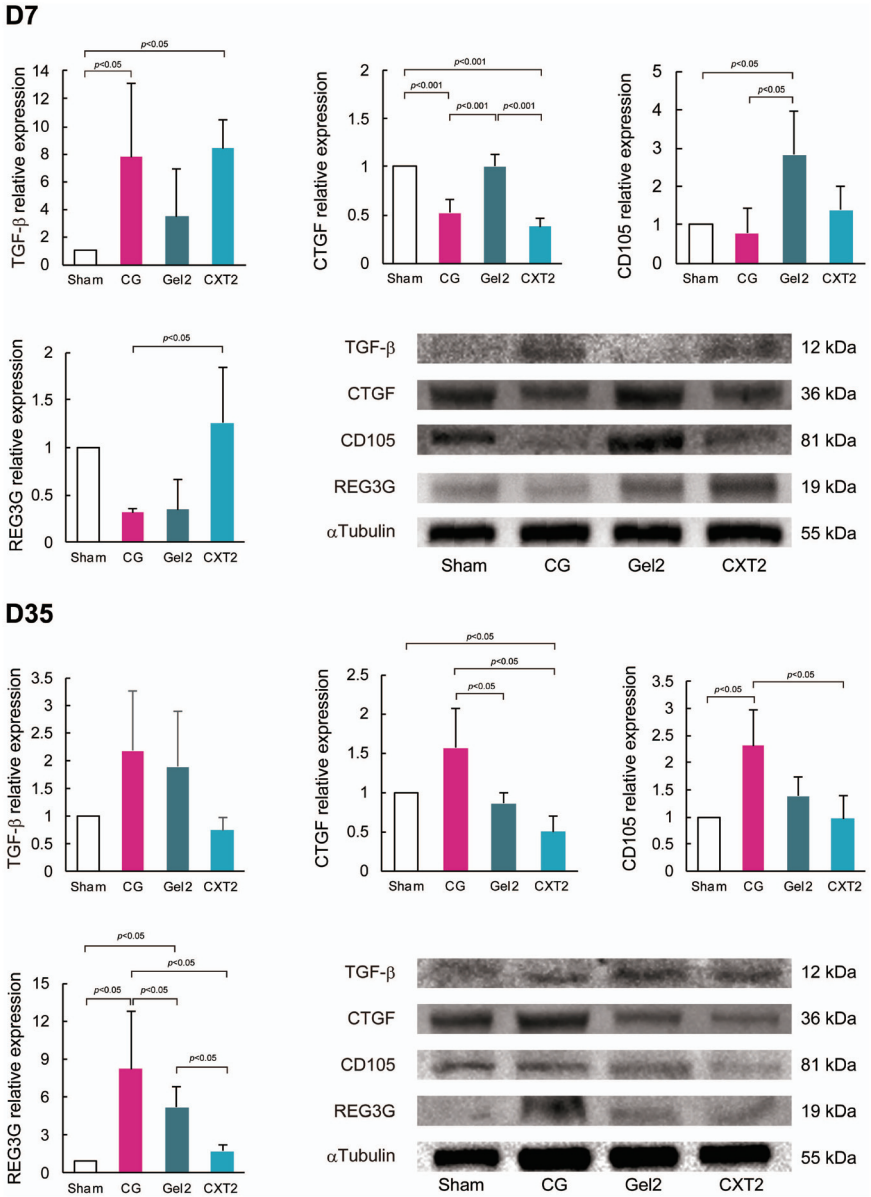

Fig. 8 Western blotting analyses of fibrosis-associated and homeostatic proteins at days 7 and 35. At day 7, the CG and CXT2 groups show significantly higher TGF-β expression compared with the Sham and Gel2 groups. The CG and CXT2 groups have significantly lower CTGF expression than the Sham and Gel2 groups. The Gel2 group shows significantly higher CD105 expression than the Sham and CG groups. REG3G expression in the CXT2 group is significantly higher than that in the CG group. At day 35, there are no differences in TGF-β expression among the groups. The CG group shows higher CTGF expression than the Gel2 and CXT2 groups. The CXT group has significantly lower CTGF expression than the other groups. The CG group shows higher CD105 expression than the Sham and CXT2 groups. The CG group exhibits higher REG3G expression than the other groups. The CXT group shows lower REG3G expression than the Gel2 group.

induce fibroblast-to-myofibroblast differentiation and extracellular matrix production.[29,30] The fibroblast-to-myofibroblast phenotypic change is a key event in tissue repair and pathological scarring.[15] CD105, a receptor for TGF-β, is highly expressed in organs undergoing angiogenesis.[31] CD105 is recognized to antagonize the inhibitory effects of TGF-β1 on vascular endothelial cells and control the formation of new blood vessels. We previously established an artificial skin and an esophageal stricture prevention patch based on collagen vitrigel, and demonstrated that these biomaterials can inhibit scar formation and inflammation through TGF-β and CTGF.[12,13] Based on these findings, we speculate that collagen vitrigel devices may have universal inhibitory effects on pathological fibrosis and inflammation in damaged organs. Contrary to our hypothesis, the CXT and CG groups had similar TGF-β and CTGF expression levels that differed from the Gel group in the early stage, but only the CXT group showed the inhibition of excess myofibroblast emergence and

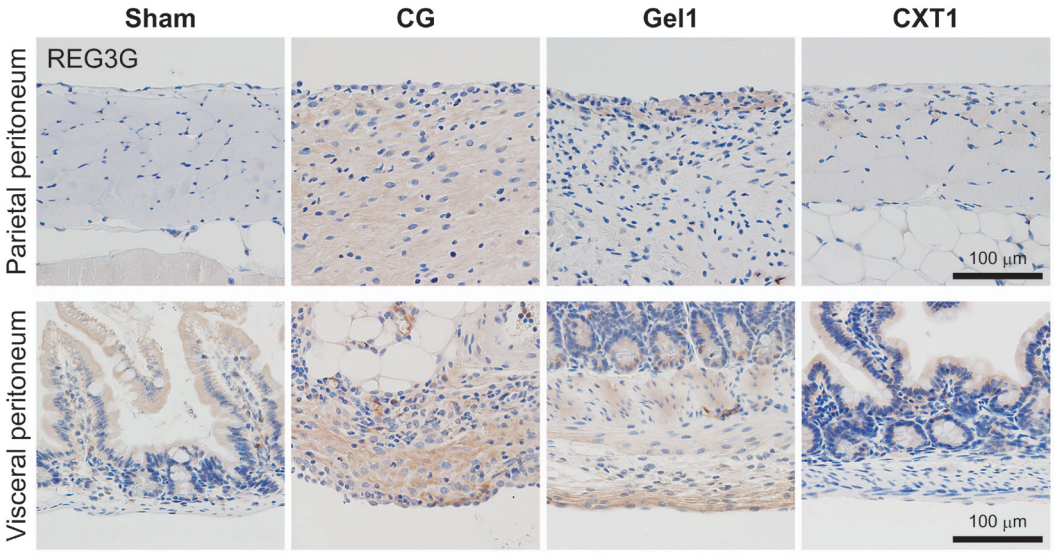

Fig. 9 Immunostaining of REG3G. The Sham and CXT1 groups contain REG3G-expressing small intestinal epithelial cells. In the CG group, REG3G-positive cells are located in the fibrotic area in both the parietal and visceral peritoneum. The Gel1 group shows REG3G-positive cells in the surface fibrotic area in both the parietal and visceral peritoneum and among small intestinal mucosal epithelial cells and smooth muscle cells.

inflammatory cell infiltration in the injured peritoneum for an extended period. In addition, the CXT and Gel groups exhibited different enhancement effects on CD105 expression in the early and late phases. These switching behaviors of CTGF and CD105 that differ from TGF-β may reflect an important role in peritoneal inflammation and fibrosis.

Intestinal epithelial cells and Paneth cells produce antimicrobial proteins and serve as the first line of defense against pathogens. The antimicrobial protein REG3G is secreted with C-type lectins and located in the gastrointestinal tract.[24] REG3G is proposed to have a protective role against infection through its bactericidal effect on Gram-positive bacteria, and controls the spatial segregation of intestinal bacteria between the inner cavity and outer body.[32,33] Loss of REG3G function was identified as a factor for the decreased spatial separation of commensals from the small intestinal epithelium in REG3G-knockout mice.[34] Cirrhotic rats showed reduced expression of *Reg3g* in the small intestine and exhibited bacterial translocation.[35] In this study, REG3G expression in the CXT group was not suppressed by CG-induced peritonitis in the early stage, and the atelocollagen gel infusion did not maintain REG3G expression. In the late phase, REG3G expression in the CG and Gel2 groups was higher than that in the CXT group, while the Sham and CXT groups showed no difference in REG3G expression. These findings suggest that a protective mechanism may be required in the peritoneum and intestine under active inflammation.

Regrettably, we were unable to clarify the precise mechanism for the anti-fibrotic and anti-inflammatory effects of CXT in this study. As described above, CXT was made from porcine-derived atelocollagen that contained types I and III collagen. Volk and colleagues[36,37] reported that type III collagen is a critical regulator of myofibroblast kinetics. They demonstrated that a shortage of type III collagen leads to the acceleration of pathological wound contraction with increased α-SMA-positive myofibroblasts. Our preliminary study on skin regeneration showed that a xerogel membrane containing types I and III collagen inhibited the emergence of myofibroblasts, while a xerogel membrane containing only type I collagen did not (data not shown). The peritoneum adjacent to the CXT showed less fibrotic change than the non-adjacent peritoneum (Fig. 5C3). These findings suggest that the distance from the tissue to the CXT may be important for the CXT to exert its protective effect. Tissue fibroblasts easily invade into the atelocollagen gel and can remodel its state, and the atelocollagen gel did not inhibit peritoneal fibrosis at day 70 (Fig. 5D2 and F). In contrast, only a small number of fibroblasts invaded into the marginal area of the CXT (Fig. 5E), and the remodeling area was limited to the CXT surface (Fig. 5G). A high-density CXT can stably retain its physical properties and may have a long-acting effect when compared with the porous gel state *in vivo*. For these reasons, we surmise that slow and sustained provision of extraneous type III collagen may inhibit pathological fibrosis and thereby protect injured tissues against pathogens.

In this study, we demonstrated the potential of a collagen xerogel thread to be developed as a new therapeutic biomaterial for the treatment of PD, but many problems remain to be solved before its clinical use. The precise mechanism of its long-term anti-fibrosis and anti-inflammation effects is a quite important issue to resolve. Additionally, denatured collagen has a risk of adverse effects, such as inflammation and peritoneal fibrosis. As shown in Fig. 4G, a small proportion of the implanted CVT exhibited a mild collagen degeneration, but the gel form of atelocollagen did not display any degenerative change. These findings suggest that further optimization of

both product quality and clinical usage will be necessary to avoid adverse effects arising from CXT treatment. Further extensive studies are needed to confirm these ideas.

Summary and conclusion

In conclusion, we have developed a novel thread type of atelocollagen xerogel that successfully prevented peritoneal fibrosis and intestinal adhesion in mice with CG-induced peritonitis. Although further work will be necessary to develop it into a clinically useful medical tool, this easy-to-handle collagen device may support desirable peritoneal homeostasis and has the potential to become a common medical tool for treating PD.

Conflicts of interest

The authors declare no potential conflicts of interest.

Acknowledgements

This work was supported in part by the Center for Clinical and Translational Research of Kyushu University Hospital (to S. A.) and by the START program (No. ST273010TT) of the Japan Science and Technology Agency (to T. T.). We thank M. Nishida, F. Mutoh, S. Nakahara, and I. Nanbu for excellent technical assistance. We are grateful to Mr K. Tokaichi for refining the English of the manuscript. We also thank Alison Sherwin, PhD, from Edanz Group for editing a draft of the manuscript.

References

1 T. A. Wynn, *J. Clin. Invest.*, 2007, **117**, 524–529.
2 J. W. Dobbie, *Peritoneal Dial. Int.*, 1992, **12**, 14–27.
3 A. M. Summers, M. J. Clancy, F. Syed, N. Harwood, P. E. Brenchley, T. Augustine, H. Riad, A. J. Hutchison, P. Taylor and R. Pearson, *Kidney Int.*, 2005, **68**, 2381–2388.
4 K. Kawanishi, K. Honda, M. Tsukada, H. Oda and K. Nitta, *Peritoneal Dial. Int.*, 2013, **33**, 242–251.
5 S. Yung and T. M. Chan, *Peritoneal Dial. Int.*, 2003, **23**(Suppl 2), S37–S41.
6 T. Takezawa, S. Aoki, A. Oshikata, C. Okamoto, H. Yamaguchi, Y. Narisawa and S. Toda, In 24th European Conference on Biomaterials (International Proceedings Division, Ed.), 2012, pp. 181–185.
7 T. Takezawa, K. Ozaki, A. Nitani, C. Takabayashi and T. Shimo-Oka, *Cell Transplant.*, 2004, **13**, 463–473.
8 H. Maruki, M. Sato, T. Takezawa, Y. Tani, M. Yokoyama, T. Takahashi, E. Toyoda, E. Okada, S. Aoki, J. Mochida and Y. Kato, *J. Biomed. Mater. Res., Part B*, 2017, **105**, 2592–2602.
9 J. Yoshida, A. Oshikata-Miyazaki, S. Yokoo, S. Yamagami, T. Takezawa and S. Amano, *Invest. Ophthalmol. Visual Sci.*, 2014, **55**, 4975–4981.
10 Y. Nakaegawa, R. Nakamura, Y. Tada, R. Suzuki, T. Takezawa, T. Nakamura and K. Omori, *Acta Otolaryngol.*, 2017, **137**, 627–634.
11 T. Takezawa, A. Nitani, T. Shimo-Oka and Y. Takayama, *Cells Tissues Organs*, 2007, **185**, 237–241.
12 S. Aoki, T. Takezawa, S. Ikeda, Y. Narisawa, A. Oshikata-Miyazaki, S. Miyauchi, H. Hirayama, T. Sawaguchi, T. Chimuro and S. Toda, *Wound Repair Regen.*, 2015, **23**, 819–829.
13 S. Aoki, Y. Sakata, R. Shimoda, T. Takezawa, A. Oshikata-Miyazaki, H. Kimura, M. Yamamoto, R. Iwakiri, K. Fujimoto and S. Toda, *Gastrointest. Endosc.*, 2017, **85**, 1076–1085.
14 K. Honda, C. Hamada, M. Nakayama, M. Miyazaki, A. M. Sherif, T. Harada and H. Hirano, *Clin. J. Am. Soc. Nephrol.*, 2008, **3**, 720–728.
15 G. Gabbiani, *J. Pathol.*, 2003, **200**, 500–503.
16 J. L. Barnes and Y. Gorin, *Kidney Int.*, 2011, **79**, 944–956.
17 L. S. Aroeira, A. Aguilera, J. A. Sánchez-Tomero, M. A. Bajo, G. del Peso, J. A. Jiménez-Heffernan, R. Selgas and M. López-Cabrera, *J. Am. Soc. Nephrol.*, 2007, **18**, 2004–2013.
18 T. Ochiya, Y. Takahama, S. Nagahara, Y. Sumita, A. Hisada, H. Itoh, Y. Nagai and M. Terada, *Nat. Med.*, 1999, **5**, 707.
19 Y. Ishii, T. Sawada, A. Shimizu, T. Tojimbara, I. Nakajima, S. Fuchinoue and S. Teraoka, *Nephrol., Dial., Transplant.*, 2001, **16**, 1262–1266.
20 Y. Yoshio, M. Miyazaki, K. Abe, T. Nishino, A. Furusu, Y. Mizuta, T. Harada, Y. Ozono, T. Koji and S. Kohno, *Kidney Int.*, 2004, **66**, 1677–1685.
21 C. T. Rueden, J. Schindelin, M. C. Hiner, B. E. DeZonia, A. E. Walter, E. T. Arena and K. W. Eliceiri, *BMC Bioinf.*, 2017, **18**, 529.
22 A. Leask and D. J. Abraham, *FASEB J.*, 2004, **18**, 816–827.
23 Q. Wang, W. Usinger, B. Nichols, J. Gray, L. Xu, T. W. Seeley, M. Brenner, G. Guo, W. Zhang and N. Oliver, *Fibrog. Tissue Repair*, 2011, **4**, 4.
24 S. Vaishnava, M. Yamamoto, K. M. Severson, K. A. Ruhn, X. Yu, O. Koren, R. Ley, E. K. Wakeland and L. V. Hooper, *Science*, 2011, **334**, 255–258.
25 L. Wang, D. E. Fouts, P. Stärkel, P. Hartmann, P. Chen, C. Llorente, J. DePew, K. Moncera, S. B. Ho and D. A. Brenner, *Cell Host Microbe*, 2016, **19**, 227–239.
26 T. Liakakos, N. Thomakos, P. M. Fine, C. Dervenis and R. L. Young, *Dig. Surg.*, 2001, **18**, 260–273.
27 Q. Zhou, M.-A. Bajo, G. del Peso, X. Yu and R. Selgas, *Kidney Int.*, 2016, **90**, 515–524.
28 D. E. Beck, Z. Cohen, J. W. Fleshman, H. S. Kaufman, H. van Goor, B. G. Wolff and C. Adhesion Study Group Steering, *Dis. Colon Rectum*, 2003, **46**, 1310–1319.
29 G. R. Grotendorst, H. Rahmanie and M. R. Duncan, *FASEB J.*, 2004, **18**, 469–479.
30 Q. Garrett, P. T. Khaw, T. D. Blalock, G. S. Schultz, G. R. Grotendorst and J. T. Daniels, *Invest. Ophthalmol. Visual Sci.*, 2004, **45**, 1109–1116.

31 C. Li, I. N. Hampson, L. Hampson, P. Kumar, C. Bernabeu and S. Kumar, *FASEB J.*, 2000, **14**, 55–64.
32 L. M. Loonen, E. Stolte, M. T. Jaklofsky, M. Meijerink, J. Dekker, P. Van Baarlen and J. Wells, *Mucosal Immunol.*, 2014, **7**, 939.
33 R. L. Gallo and L. V. Hooper, *Nat. Rev. Immunol.*, 2012, **12**, 503.
34 S. Vaishnava, M. Yamamoto, K. M. Severson, K. A. Ruhn, X. Yu, O. Koren, R. Ley, E. K. Wakeland and L. V. Hooper, *Science*, 2011, **334**, 255–258.
35 Z. Teltschik, R. Wiest, J. Beisner, S. Nuding, C. Hofmann, J. Schoelmerich, C. L. Bevins, E. F. Stange and J. Wehkamp, *Hepatology*, 2012, **55**, 1154–1163.
36 B. K. Brisson, E. A. Mauldin, W. Lei, L. K. Vogel, A. M. Power, A. Lo, D. Dopkin, C. Khanna, R. G. Wells, E. Pure and S. W. Volk, *Am. J. Pathol.*, 2015, **185**, 1471–1486.
37 S. W. Volk, Y. Wang, E. A. Mauldin, K. W. Liechty and S. L. Adams, *Cells Tissues Organs*, 2011, **194**, 25–37.